

Article title: Ferulic acid enhances the radiation sensitivity of lung and liver carcinoma cells by collapsing redox homeostasis: mechanistic link of Akt/p38 MAPK signalling pathway

Name of the Authors:

Ujjal Das¹, Krishnendu Manna², Arghya Adhikary³, Snehasis Mishra², Krishna Das Saha², Rakhi Dey Sharma⁴, Biswanath Majumder^{5*} and Sanjit Dey^{1*}

Affiliations:

¹Department of Physiology, Centre for Nanoscience and Nanotechnology and Centre with Potential for Excellence in Particular Area (CPEPA), University of Calcutta, 92 APC Road, Kolkata-700009, India,

²Cancer Biology and Inflammatory Disorder Division, CSIR-Indian Institute of Chemical Biology, 4, Raja S.C. Mullick Road, Kolkata-700032, West Bengal, India.

³Centre for Nanoscience and Nanotechnology (CRNN), University of Calcutta, Salt Lake, Kolkata-700098

⁴Barrackpore Rastraguru Surendranath College, 85 Middle Road, Barrackpore, Kolkata-700120, India

⁵Department of Molecular Pathology and Cancer Biology, Mitra Biotech, 202, Narayana Nethralaya, Hosur Main Road, Bangalore 560099, India

Name and contact information of corresponding author:

Name: **Professor Sanjit Dey**

Address: Department of Physiology, 92 APC Road, Kolkata 700 009, West Bengal, India

Telephone: +91-9830211512

E-mail: **sanjitdey@gmail.com**

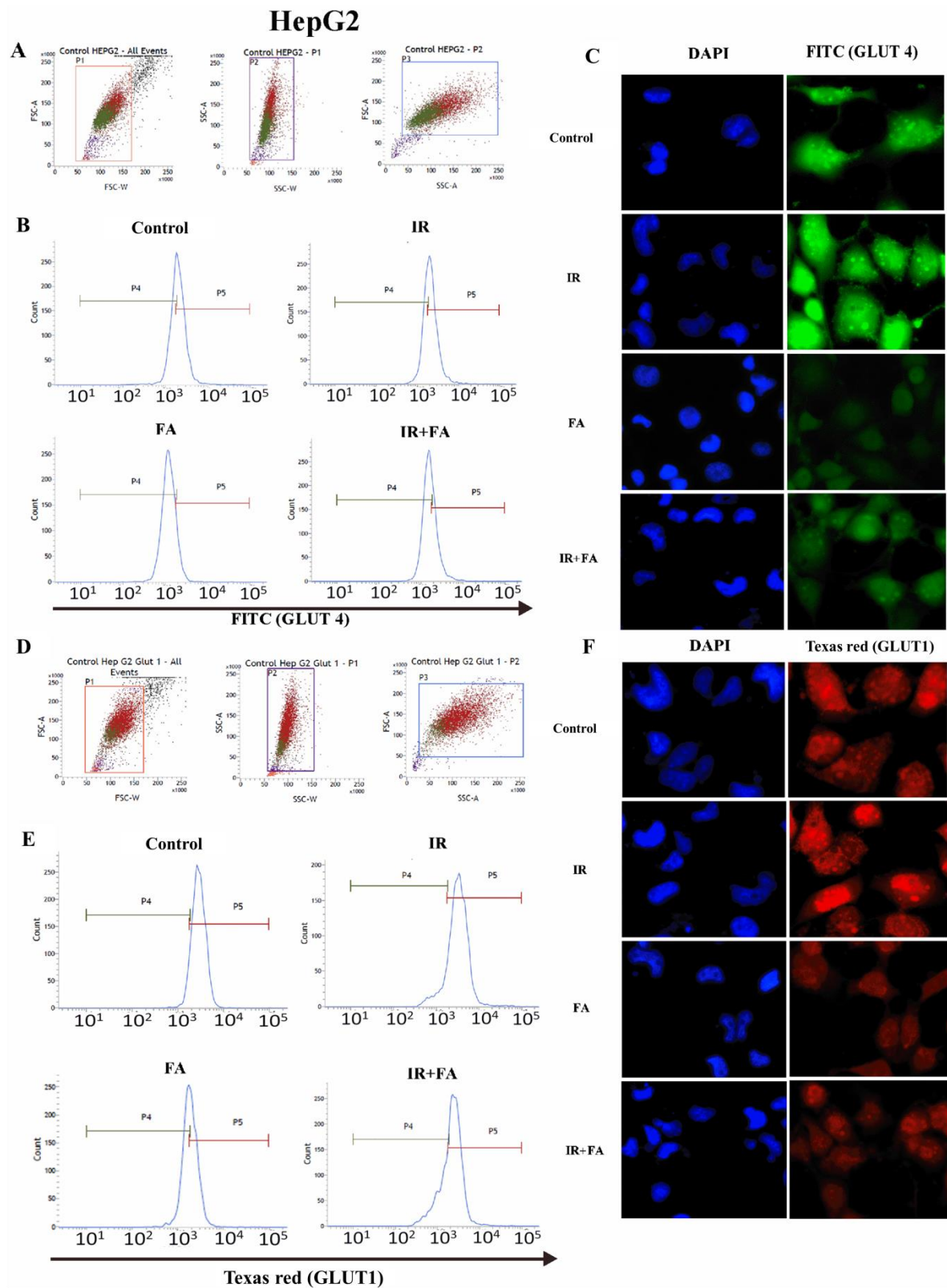
Name: **Dr. Biswanath Majumder**

E-mail: **bmajumder@mitrabiotech.com**

Key words: Ferulic acid; γ -radiation, Carcinoma cells; radiation sensitization; Tumour regression.

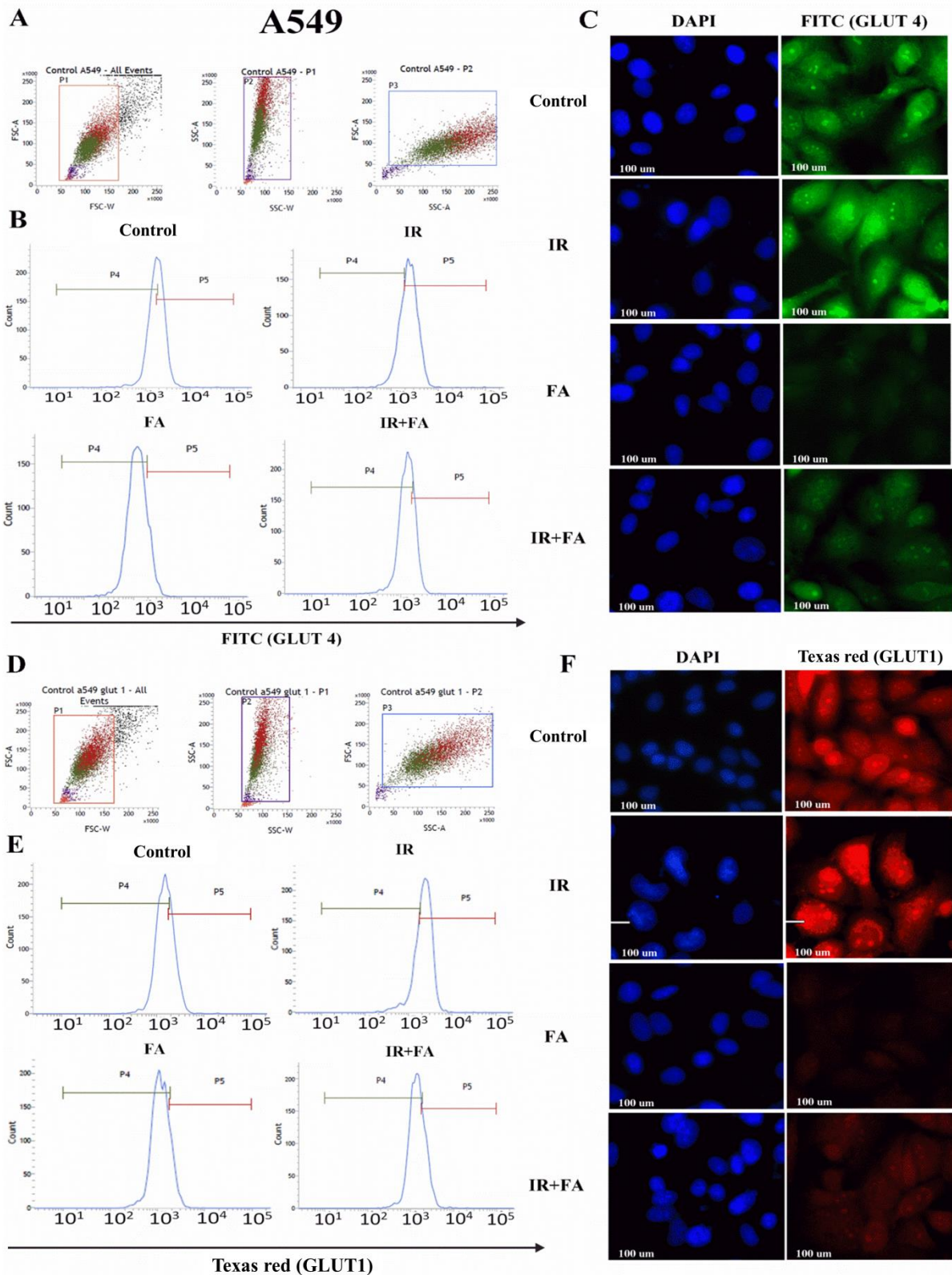
Running Title: Ferulic acid induces radiosensitization

FA decreased the expression of GLUT1 and GLUT4 in both HepG2 and A549 cells



Supplementary figure 1: Effect of FA treatment on GLUT 4 and GLUT 1 expression in HepG2 cells. A. The dot plots indicate the separation of cell debris from actual population. **B.** Histogram plots show the level of GLUT 4 in different experimental groups **C.** The

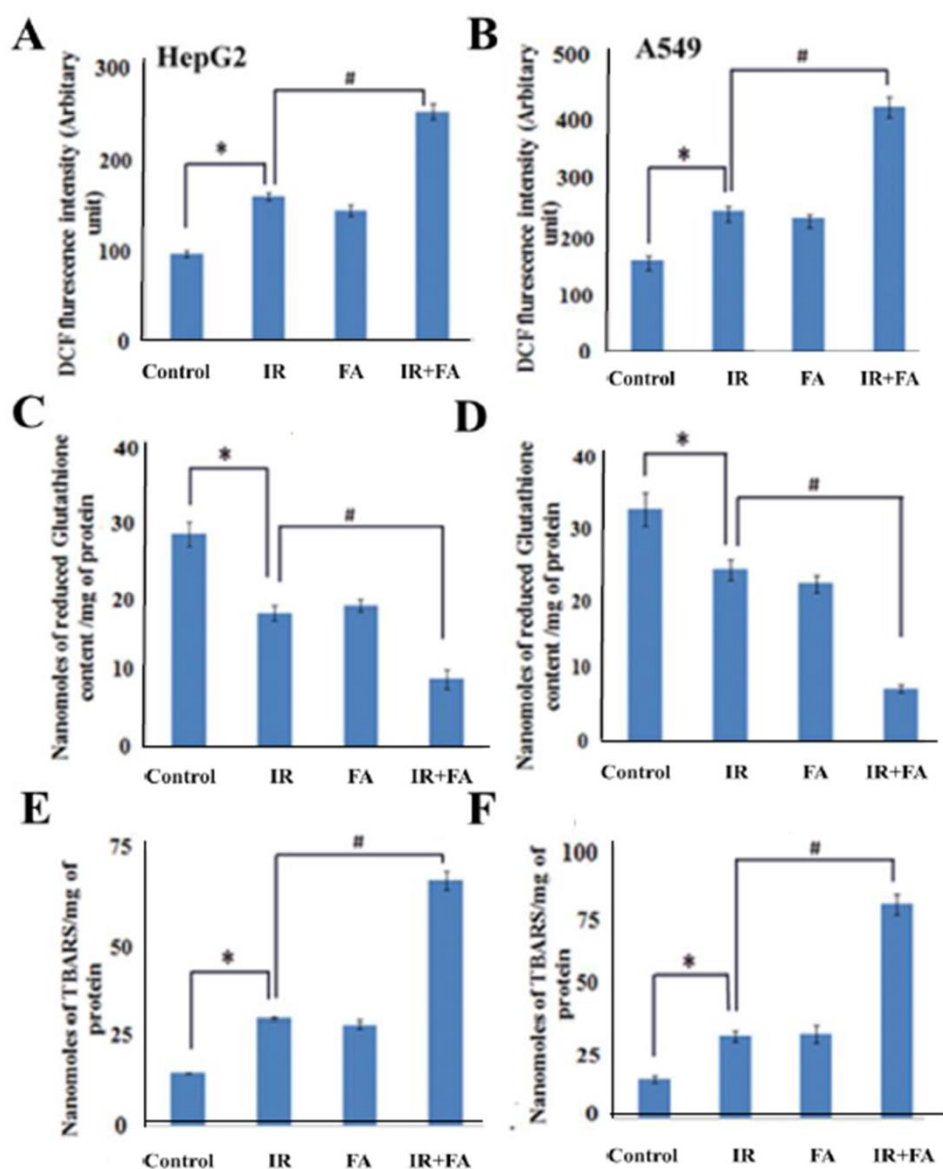
immunocytochemistry study of GLUT 4. The nuclei were stained by DAPI and GLUT 4 was stained by FITC tagged secondary antibody. **D.** The diagram shows the dot plot of GLUT 1. **E.** The histogram plots represent the expression of GLUT 1 in HepG2 cells. **F.** The immunocytochemistry study of GLUT 1. The nuclei were stained by DAPI and GLUT 1 is stained by texas red tagged secondary antibody.



Supplementary figure 2: Effect of FA treatment on GLUT 4 and GLUT 1 expression in A549 cells. **A.** The dot plots show the separation of debris from actual cell population. **B.** Histogram plots show the level of GLUT 4 in different experimental groups. **C.** The immunocytochemistry study of GLUT 4. The nuclei were stained by DAPI and GLUT 4 was stained by FITC tagged secondary antibody. **D.** The diagram shows the dot plot of GLUT 1. **E.** The histogram plots represent the expression of GLUT 1 in A549 cells. **F.** The immunocytochemistry study of GLUT 1. The nuclei were stained by DAPI and GLUT 1 was stained by texas red tagged secondary antibody.

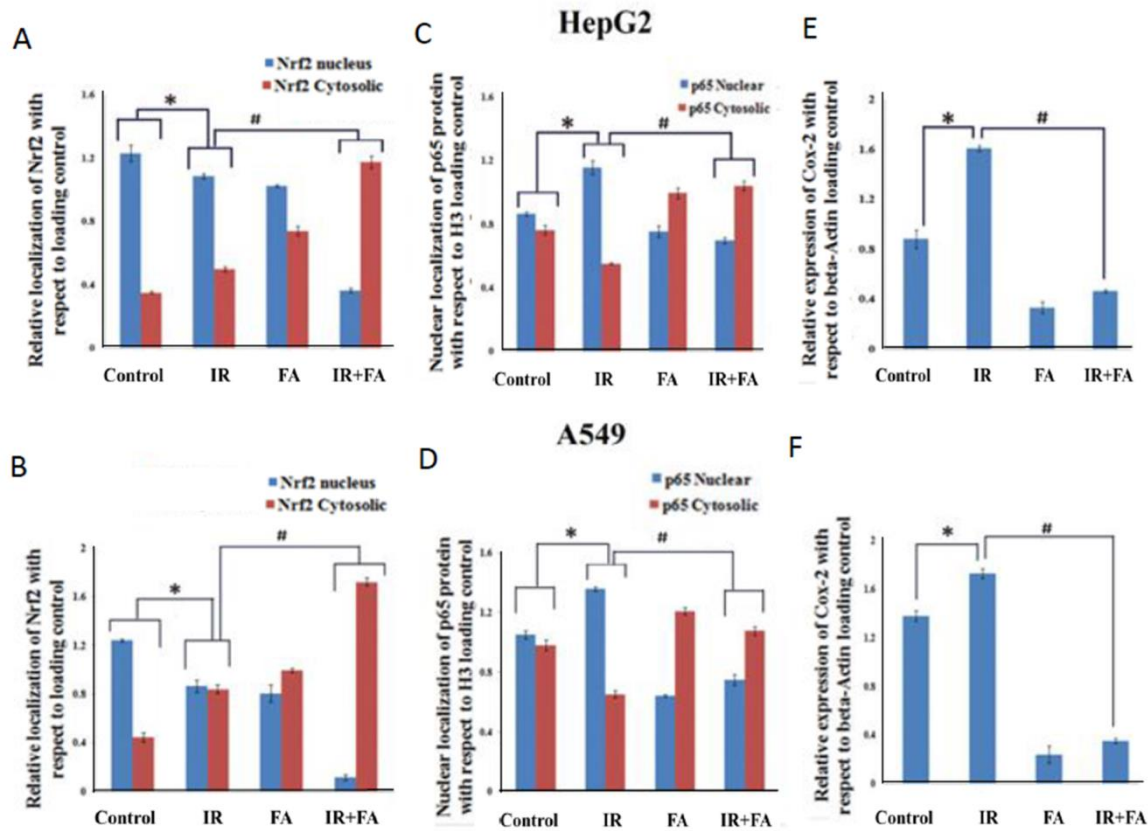
Cancer cells depend mainly on glucose metabolism for their energy production and macromolecular synthesis. Even under aerobic conditions, tumour cells continue to rely on glycolysis rather than oxidative phosphorylation (Warburg effect), resulting in high glucose requirements to generate energy and support metabolic function. Therefore, the presence of GLUT1 and GLUT4 on cell surface and their expression were measured by immunocytochemistry and flowcytometry respectively (S1 & 2). The fluorescence intensity of FITC and texas red (TR) was increased by irradiation indicating the higher surface level of GLUT 4 (FITC) and GLUT 1 (TR) in both HepG2 and A549 cells. The histogram plot of flowcytometry data further showed the higher expression of these transporters in irradiated groups compared to control (S1 A-F & 2 A-F). One potential explanation is that radiation induces cellular stress which triggers the up regulation and trafficking of these proteins to cell surface to increase glucose uptake and energy production rate. This strategy confers radioresistance property to cancer cells. Interestingly, FA treatment decreased the level of GLUT 4 and GLUT 1 in HepG2 cells by 2.0 and 1.8 fold respectively compared to control (S1). The treatment with FA also decreased the GLUT 4 and GLUT 1 level in A549 cells by 3.5 and 2.9 folds respectively compared to control (S2). Therefore, the surface intensity of GLUT also decreased. Combination of IR and FA showed higher level of GLUT 4 and GLUT 1 expression compared to FA treatment alone, the level of GLUT 1 and GLUT 4 was significantly ($p < 0.05$) lower than irradiated groups. Thus, it may block the entry of glucose followed by glycolysis.

Combination of IR and FA treatment increased oxidative damage



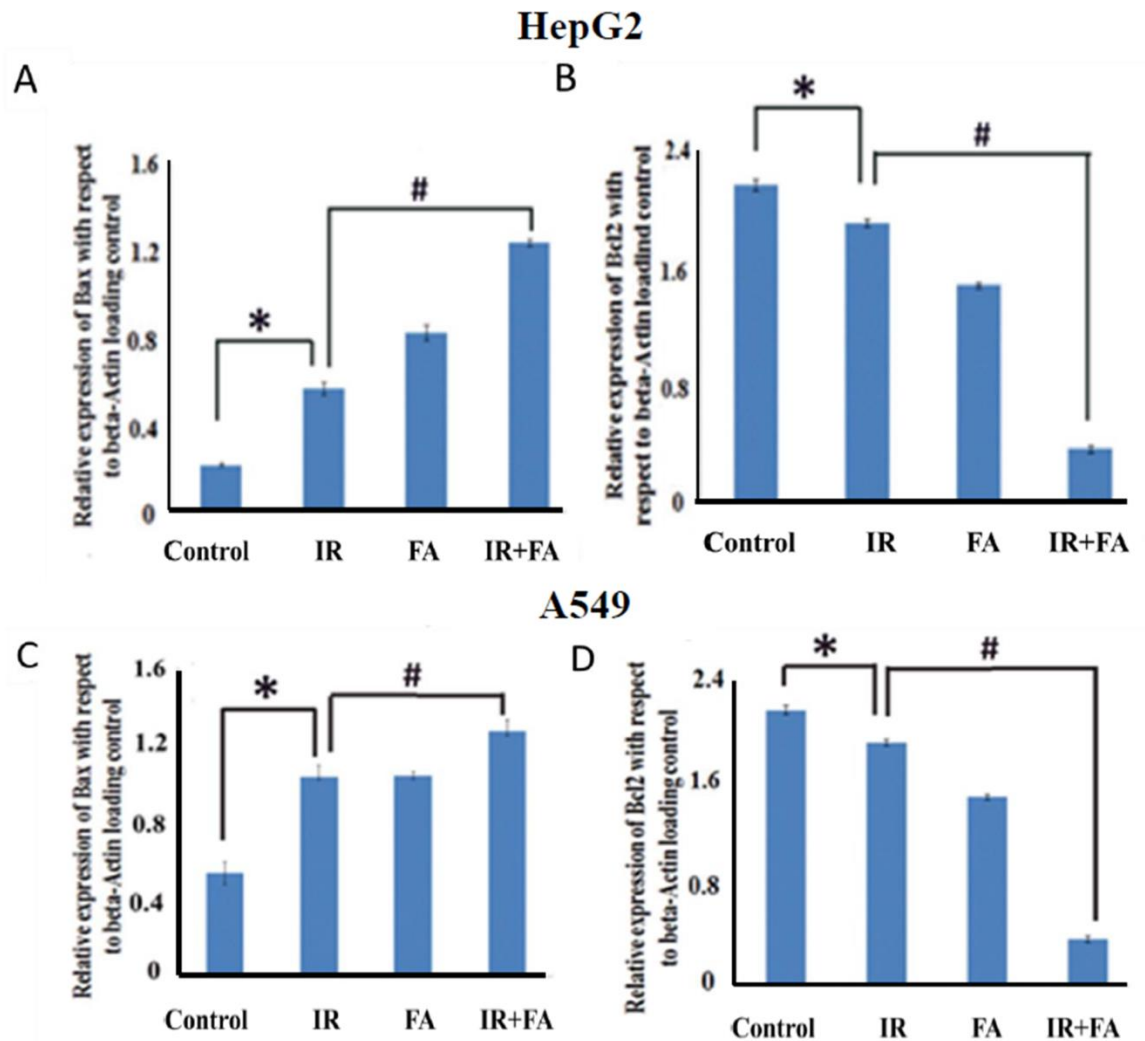
Supplementary figure 3. Effect of combination treatment on cellular redox state: **A.** The bar diagram represents the mean fluorescence intensity of DCF in HepG2 cells. IR+FA group shows highest DCF fluorescent intensity among all other groups. **B.** The bar diagram represents the mean fluorescence intensity of DCF in A549 cells. **C.** Bar diagram represents the reduced glutathione content in control, IR, FA and IR+FA treated groups of HepG2 cells. **D.** Bar diagram represents the reduced glutathione content in control, IR, FA and IR+FA treated A549 cells. Nano moles of reduced glutathione/mg of protein were plotted along the Y-axis and Control, IR, FA and IR+FA were taken along the X-axis. **E.** Bar diagram represents the TBARS level in Control, IR, FA and IR+FA treated HepG2 cells. **F.** Bar diagram represents the TBARS level in Control, IR, FA and IR+FA treated A549 cells. Nano moles of TBARS/ mg of protein were plotted along the Y-axis and Control, IR, FA and IR+FA were taken along the X-axis. Error bars are SEM for n=3. $p < 0.05$ was considered significant. Statistical comparison was done between control vs. IR designated by ‘*’, and IR vs. FA + IR designated by ‘#’ in figure.

Combination treatment inhibited nuclear translocation of NF- κ B/p65 and Nrf2 transcription factors



Supplementary figure 4. Effect of combination treatment on the nuclear translocation of NF- κ B/p65 and Nrf2 in A549 and HepG2 cells: **A.** The figure shows the densitometric analysis of nuclear localization of Nrf2 in HepG2 cells. According to the Y-axis relative localization of Nrf2 was taken and along the X-axis different experimental groups were plotted. **B.** The figure shows the densitometric analysis of nuclear localization of Nrf2 in A549 cells. According to the Y-axis relative localization of Nrf2 was taken and along the X-axis different experimental groups were plotted. **C.** The diagram represents the densitometric analysis of nuclear and cytosolic localization of NF- κ B/p65 in different experimental groups in HepG2 cells. **D.** The diagram represents the densitometric analysis of nuclear and cytosolic localization of NF- κ B/p65 in different experimental groups in A549 cells. **E.** The figure shows the relative expression of Cox-2 in HepG2 cells under different experimental conditions. **F.** The figure shows the relative expression of Cox-2 in A549 cells under different experimental conditions. The image J 1.42q was used to quantify the immunoblot band. Error bars are SEM for n=4. $p < 0.05$ were considered significant. Statistical comparison was done between control vs. IR designated by ‘*’, and IR vs. FA + IR designated by ‘#’ in figure.

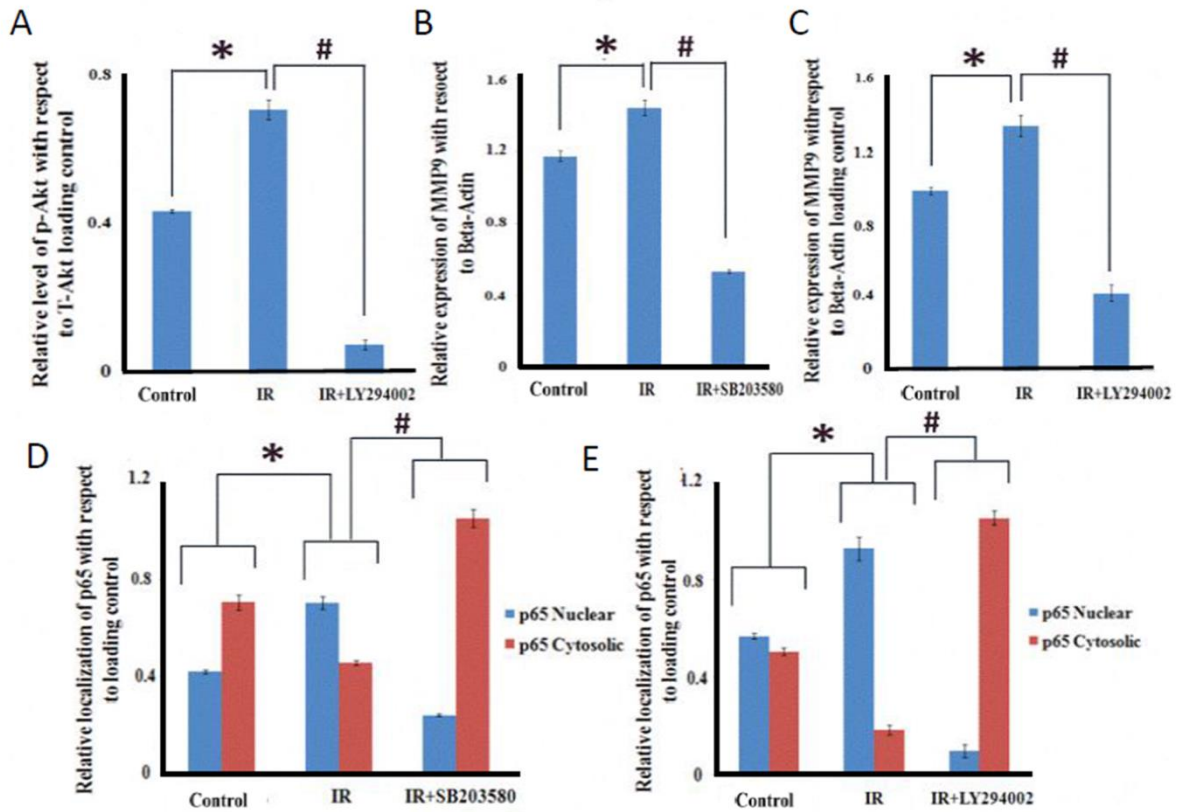
FA and IR combination treatment increased Bax/Bcl2 ratio in both the carcinoma cells



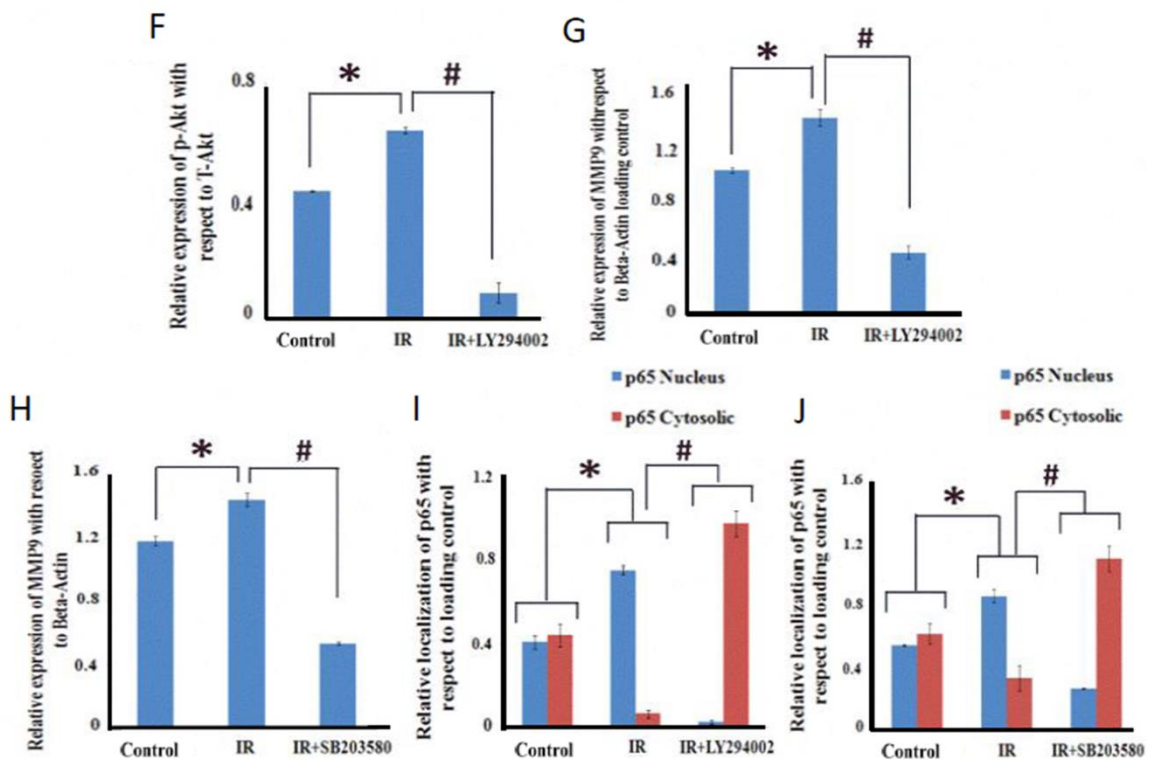
Supplementary figure 5. Effect of combination treatment on Bax/Bcl2 ratio in HepG2 and A549 cells: **A.** The figure shows the densitometric analysis of Bax expression in HepG2 cells. According to the Y-axis relative expression of Bax was taken and along the X-axis different experimental groups were plotted. **B.** The diagram represents the densitometric analysis of Bcl2 expression in different experimental groups in HepG2 cells. **C.** The figure shows the relative expression of Bax in A549 cells under different experimental conditions. **D.** The figure shows the relative expression of Bcl-2 in A549 cells under different experimental conditions. The image J 1.42q was used to quantify the immunoblot bands. Error bars are SEM for n=4. $p < 0.05$ was considered significant. Statistical comparison was done between control vs. IR designated by ‘*’, and IR vs. FA + IR designated by ‘#’ in figure.

Confirmation of signalling pathway involved

HepG2



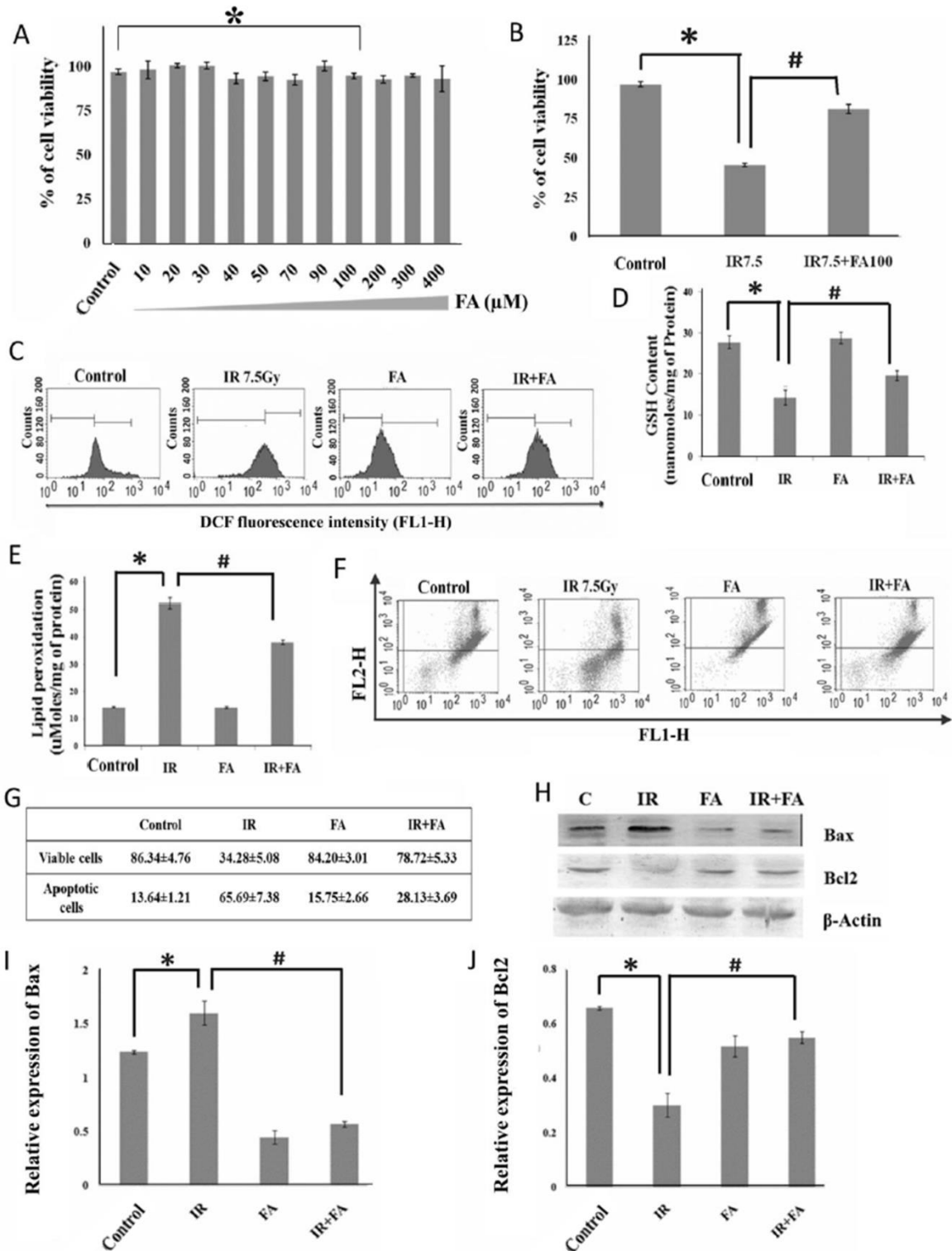
A549



Supplementary figure 6. Signal transduction pathways involve in radiation induced enhanced expression of MMP-9 in HepG2 and A549 cells. **A.** The bar diagram represents the p-Akt level under different experimental conditions in HepG2 cells. **B.** The figure represents the densitometric analysis of MMP-9 immunoblot in presence of LY294002 inhibitor in HepG2 cells. **C.** The figure represents the densitometric analysis of MMP-9 immunoblot in presence of SB203580 inhibitor in HepG2 cells. **D.** The bar diagram shows subcellular localization of p65 in presence of LY294002 inhibitor in HepG2 cells. **E.** The bar diagram shows subcellular localization of p65 in presence of SB203580 inhibitor in HepG2 cells. **F.** The bar diagram represents the p-Akt level in different experimental conditions in A549 cells. **G.** The figure represents the densitometric analysis of MMP-9 immunoblot in presence of LY294002 inhibitor in A549 cells. **H.** The figure represents the densitometric analysis of MMP-9 immunoblot in presence of SB203580 inhibitor in A549 cells. **I.** The bar diagram shows subcellular localization of p65 in presence of LY294002 inhibitor and **J.** in presence of SB203580 inhibitor in A549 cells. Data were obtained from two independent experiments. SEM for n=2. $p < 0.05$ was considered significant. Statistical comparison is done between ‘*’ control vs. IR, and ‘#’ IR vs. IR+ Inhibitor.

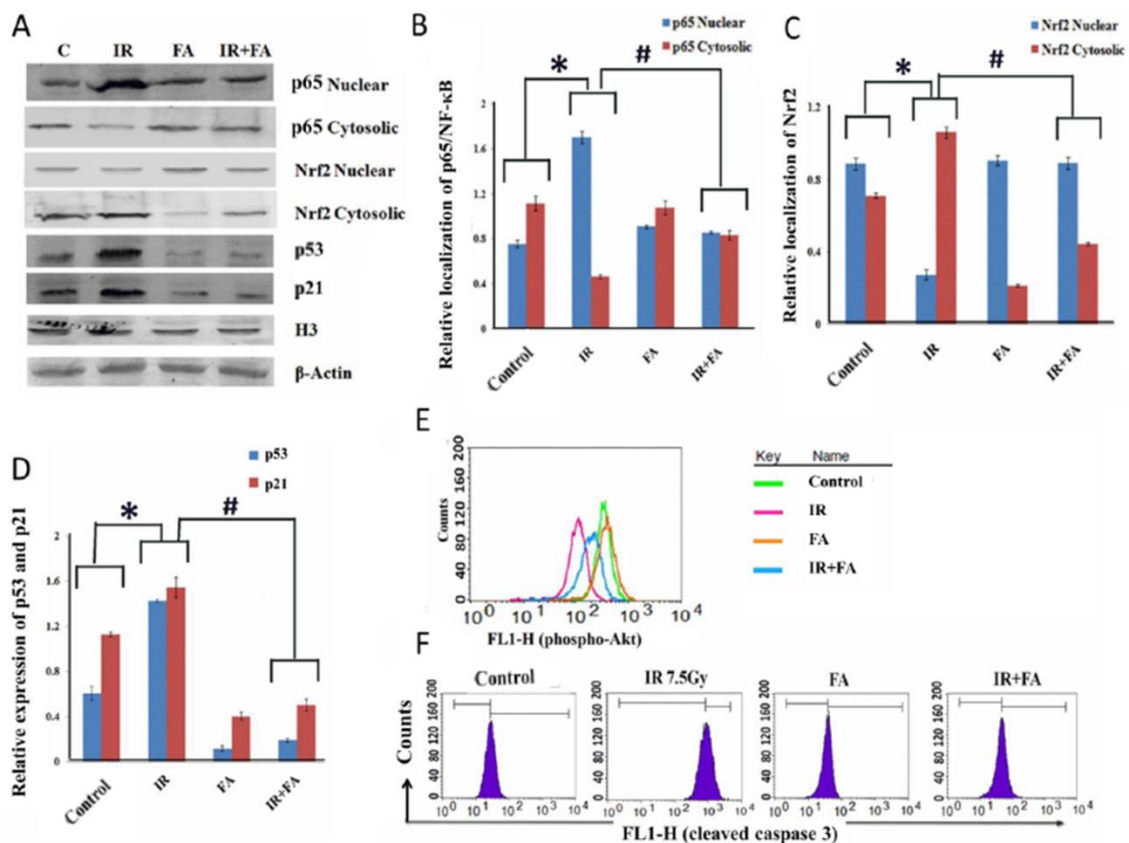
FA protected the normal PBMC cells from radiation hazards

The immune network should remain unperturbed under any treatment condition to maintain the overall normal physiological conditions to avert toxicity of drugs, if any. Thus we elucidated the effects of the same treatment arms on normal healthy PBMC which is a model of microenvironment milieu in *in vitro* system. The same dose of FA (100 μ M) did not confer any effect on PBMC viability. Moreover, pretreatment with FA prior to radiation significantly ($p < 0.05$) prevented the cell death (78.44 \pm 4.08% viable) induced by irradiation (48.78 \pm 1.76% viable) exposure (S7 A & B). Irradiation caused 2.2 fold increase in the ROS level after 1 h compared to the control PBMC. As observed in S7 C, the FA pretreatment significantly prevented the radiation induced ROS generation in PBMC. The treatment with FA not only prevented the TBARS formation by scavenging ROS, but also restored the reduced glutathione content (S7 D & E). Additionally, irradiation showed 65.69 \pm 7.38% cell population with a loss of mitochondrial membrane potential, indicating the ROS induced damage to mitochondria in PBMC. However, the FA pretreatment significantly prevented mitochondrial damage represented by 78.72 \pm 5.33% viable cells in IR+FA group (S7 F & G). The FA treatment favoured the Bcl-2 expression with the simultaneous inhibition of Bax and shifted the equilibrium towards survival (S7 H-J).



Supplementary figure 7. Effect of combination treatment on normal cell PBMC: **A.** The figure shows the percentage of PBMC survivability in presence of increasing concentration of FA. **B.** Bar diagram represents the viability of PBMC cells after radiation and IR+FA treatment. Data was obtained from 5 independent experiments. SEM for n=5. $p < 0.05$ was considered significant. **C.** The histogram plot represents the ROS level in PBMC cells under different experimental conditions. The movement of histogram towards right indicates the higher ROS generation. DCF intensity was taken along the X axis, FL1-H (green) channel

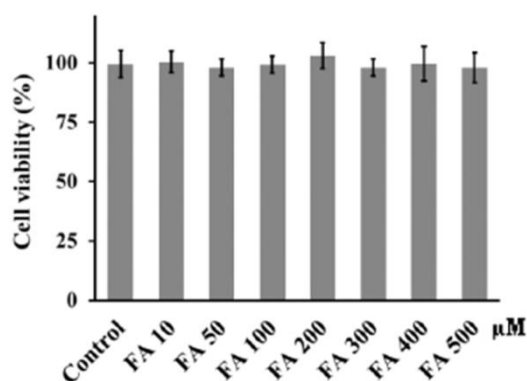
and count was taken along the Y-axis. **D.** Bar diagram represents the reduced glutathione content in control, IR, FA and IR+FA treated groups. **E.** Bar diagram represents the TBARS level **F.** Dot plots represent the alteration of mitochondrial membrane potential under different experimental conditions. The upper quadrant represents the cell population with no loss of mitochondrial membrane potential (viable population) and the lower quadrant represents the cell population with loss of mitochondrial membrane potential (apoptotic population). **G.** The table represents the percentage of viable and apoptotic population of PBMC in terms of mitochondrial membrane potential alteration. **H.** Immunoblot images show expression of Bax and Bcl-2 under different experimental conditions. **I.** The bar diagram represents the relative expression of Bax in different experimental groups. **J.** The bar diagram represents the relative expression of Bcl-2 in different experimental groups. Data was obtained from three independent experiments. SEM for n=3. $p < 0.05$ was considered significant. Statistical comparison was done between ‘*’ control vs. IR, and ‘#’ IR vs. FA + IR.



Supplementary figure 8. Effect of IR and FA combination treatment on signal transduction pathway of PBMC: **A.** The immunoblot images shows the level of p53, p21 and nuclear, cytosolic localization of p65 and Nrf2. **B.** The bar diagram represents the densitometric analysis of subcellular localization of p65 and **C.** the subcellular localization of Nrf2. **D.** The bar diagram represents the densitometric analysis of p53 and p21 under different experimental conditions. **E.** The overlapped histogram plot indicates the level of p-Akt. **F.** The overlapped histogram plot represents the cleaved caspase 3 level. Data were obtained from three independent experiments. SEM for n=3. $p < 0.05$ is considered significant. Statistical comparison was done between ‘*’ control vs. IR, and ‘#’ IR vs. FA + IR.

We also studied the nuclear localization of NF- κ B, p53 protein and Nrf2 after 24 h of irradiation. The nuclear translocation of NF- κ B and Nrf2 displayed contrasting patterns in this scenario. Irradiation to PBMC significantly increased the level of NF- κ B within the nuclei. However, irradiation caused 3.23 fold down regulation in Nrf2 nuclear localization (S8 A-C). FA treatment prior to irradiation showed a reversed effect, wherein a lower nuclear localization of NF- κ B and a concurrent increased in Nrf2 level within the nuclei was observed (S8 A-C). Interestingly, the irradiation caused 2.3 fold increase in p53 compared to the control group (S8 A & D). The pretreatment with FA prior to irradiation remarkably decreased the p53 level by 7.3 fold. Moreover, the combinatorial treatment of FA+IR of PBMC showed 3.3 fold lower expression of p21^{waf1/cip1} than the irradiated PBMC (S8 A & D). The level of p-Akt was also examined by flow cytometry after 6 h of irradiation. Irradiation reduced the p-Akt level in PBMC by 1.95 fold as shown in S8 E. The treatment of PBMC with FA increased the p-Akt level and also the survivability of PBMC. Finally, we checked the level of active caspase 3 in PBMC after 40 h of irradiation. The data in S8 F showed 3.9 fold higher level of active caspase 3 in irradiated PBMC compared to the control. The combination treatment effectively decreased the level of active caspase 3 by 3.6 fold with respect to IR alone. Therefore, the cumulative results showed that the combination of IR+FA treatment favoured the cell survival, prevented oxidative stress and stress induced apoptosis of normal PBMC.

The effect of FA treatment alone on WI-38 cells

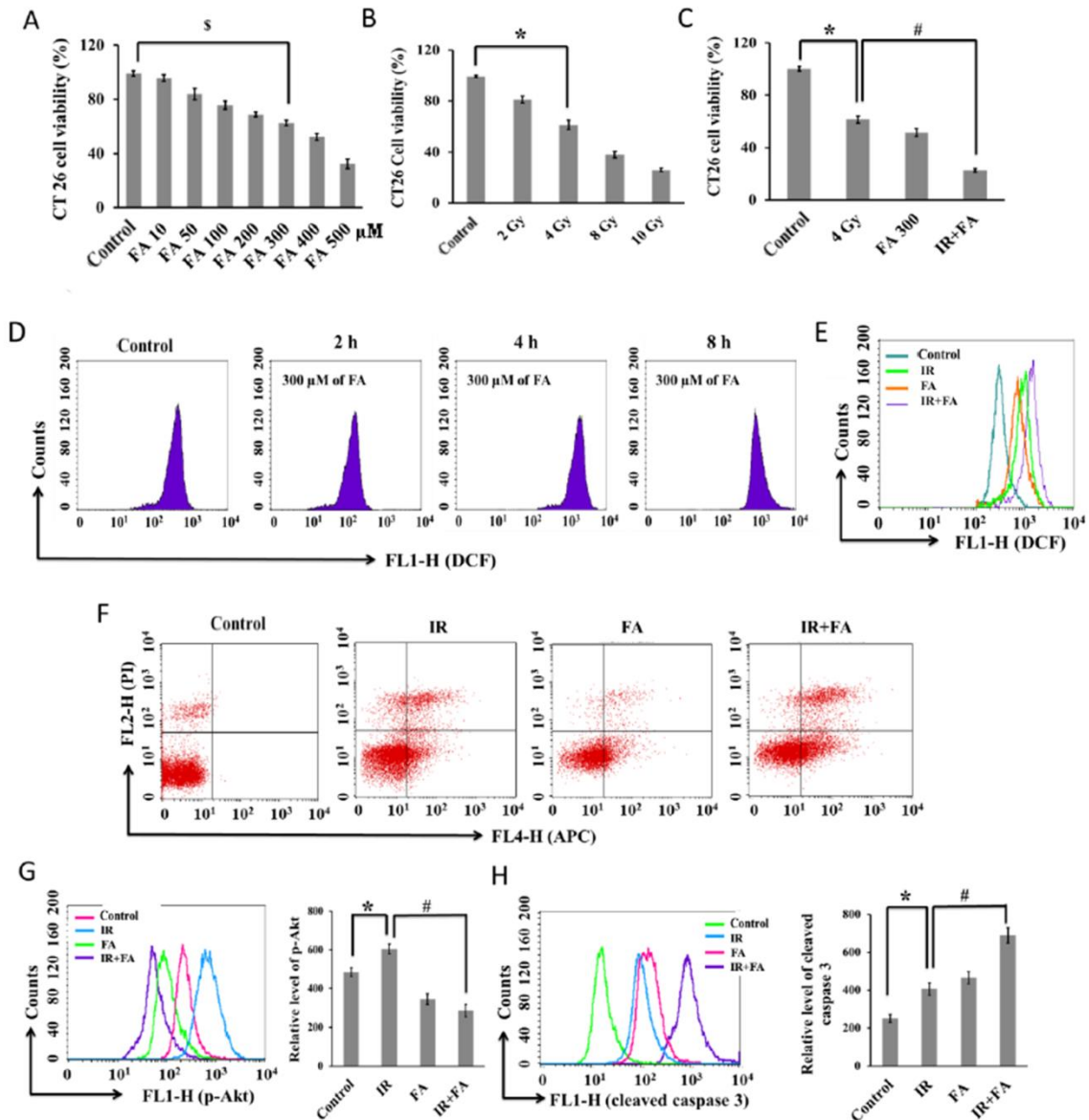


Supplementary figure 9. The figure shows the percentage of WI-38 cells viability in presence of increasing concentration of FA.

The WI-38 cells were treated with increasing concentration of FA (10-500 μ M). The cells were incubated for 72 hr then MTT assay was performed to check the cell viability. FA

treatment didn't show any toxic effect WI-38 lung fibroblast normal cells even at 500 μM dose.

Combination of FA and IR treatment increased radiation sensitivity of CT26 colon carcinoma cells



Supplementary figure 10. Effect of combination treatment on CT26 murine colon carcinoma cells: **A.** The figure shows the percentage of CT26 cells viability in presence of increasing concentration of FA. **B.** Bar diagram represents the viability of CT26 cells after exposure of different doses of radiation. **C.** Bar diagram represents the viability of CT26 cells under different treatment conditions. Data are obtained from 4 independent experiments. SEM for $n=4$. $p < 0.05$ is considered significant. **D.** The histogram plot represents the ROS level in CT26 cells under different experimental conditions. DCF intensity is taken along the X axis, FL1-H (green) channel and count is taken along the Y-axis. **E.** The histogram plot represents the ROS level in CT26 at different time points after FA (300 μM) alone treatment. **F.** Dot plots represent the PS externalization and PI incorporation in different treatment

groups. The upper right quadrant represented the late apoptotic cell populations and lower right quadrant represents the early apoptotic populations and Upper left quadrant represents the necrotic populations. **G.** The histogram plot indicates the level of p-Akt. **H.** The histogram plot indicates the active caspase 3 level. Data was obtained from 2 independent experiments. SEM for n=2. $p < 0.05$ was considered significant. Statistical comparison is done between ‘\$’ control vs. FA, ‘*’ control vs. IR, and ‘#’ IR vs. FA + IR.

With increasing concentration of FA treatment, the viability of CT26 cells was decreased gradually. The IC_{50} concentration of FA for CT26 cells was 400 μ M (Fig S10 A). Therefore, we used 300 μ M dose of FA for combination treatment. The radiation dose profile study revealed approximately 67% cells viability after 72 hr of 4 Gy irradiation (Fig S10 B). The combination of 4 Gy irradiation and 300 μ M of FA treatment reduced the cell viability to 23% and therefore, chosen for further experiments (Fig S10 C). The cells were also treated with 300 μ M of FA and were harvested at different time points just like the other cell lines (HepG2, A549, WI-38). The ROS generation was observed at different time points after FA treatment. The ROS level was significantly low after 2 hr of FA treatment but dramatically increased after 4 hr (Fig S10 D). The same result was also found for A549 (3 hr) and HepG2 (6 hr) cells in this present study. Therefore, this time point was chosen to expose the CT26 cells to 4 Gy irradiation. The combination treatment significantly increased ROS generation (Fig S10 E), percentage of early and late apoptotic population compared to radiation alone (Fig S 10 F). The increase in cleaved caspase 3 level (Fig S10 G) and suppression of Akt activation (Fig S10 H) confirmed the augmentation of death signal in CT26 cells due to the combination treatment.